Interfacial dark aging is an overlooked source of aqueous secondary organic aerosol

Fei Zhang,[a,b,c] Manh Thuong Nguyen,[d] Yao Fu,[c] and Xiao-Ying Yu[c,]*

[a] College of Environmental and Resource Sciences, Zhejiang University, Hangzhou 310058, China

[b] State Environmental Protection Key Laboratory of Formation and Prevention of Urban Air Pollution Complex, Shanghai Academy of Environment Sciences, Shanghai 200233, China

[c] Energy and Environment Directorate, Pacific Northwest National Laboratory, Richland, WA 99354, USA

[d] Physical and Computational Sciences Directorate, Pacific Northwest National Laboratory, Richland, WA 99354, USA

***Corresponding author:** Dr. Xiao-Ying Yu: xiaoying.yu@pnnl.gov; Tel: 509-372-4524; Fax: 509-375-2999

Table of Contents

Supporting Method Details

Dry reference sample preparation

The dry reference sample preparation processes follow the same procedure in our recent publication (Sui et al., 2018). First, we cleaned the Si wafer thoroughly with acetone, isopropanol, and DI water for 1 min each. Afterwards, we dried the Si wafer by N_2 gas and treated the wafers with UV-O_3 plasma (Model No.342, Jelight Company Inc., USA) for 1 min. to remove the organic residues on the wafers. Then, we prepared the samples with a concentration of 1 mg/mL in the fume hood. Finally, we dispensed the aqueous solution onto the clean Si wafer and covered the wafer with a petri dish in the fume hood during drying.

Computational methods for surface cluster ion formation

For the $H^+(H_2O)_n$ clusters (n=3,6), the binding energy was calculated Eqn. (S1),

$$E_{binding} = \frac{1}{n}[E(H^+(H_2O)_n) - (n-1)E(H_2O) - E(H^+H_2O)] \quad \text{Eqn. (S1)}$$

in which $E(H_2O)$ and $E(H^+H_2O)$ are the energy of a H_2O and H^+H_3O molecule, respectively.

Our MD calculations predict the binding energy of -81 and -70 kJ/mol for the $H^+(H_2O)_3$ and $H^+(H_2O)_6$, respectively. The binding energy per molecule was then calculated using Eqn. (S2):

$$E_{binding} = \frac{1}{4}\left[E\left(H^+(H_2O)_3(C_2H_2O_2)\right) - 2E(H_2O) - E(H^+H_2O) - E(C_2H_2O_2)\right] \quad \text{Eqn. (S2)}$$

which leads to -84 kJ/mol.

For the m/z^+ 165 $H^+C_2H_3O_3\cdots C_2H_2O_4$ cluster, the binding energy was calculated using Eqn. (S3):

$$E_{binding} = \frac{1}{2}\left[E\left(H^+(C_2H_3O_3)(C_2H_2O_4)\right) - E\left(H^+(C_2H_2O_4)\right) - E(C_2H_3O_3)\right] \quad \text{Eqn. (S3)}$$

Here the two molecular constituents $H^+C_2H_3O_3$ and $C_2H_2O_4$ were not considered at their reference states because the sum of their energies is higher than those of the two constituents $H^+C_2H_2O_4$ and $C_2H_3O_3$, respectively. In this case, the binding energy was -62 kJ/mol.

For the m/z^+ 173 $H^+C_4H_{10}O_6\cdots H_2O$ cluster, the binding energy was calculated using Eqn. (S4)

$$E_{binding} = \frac{1}{2}\left[E\left(H^+(C_4H_{10}O_6)(H_2O)\right) - E\left(H^+(C_4H_{10}O_6)\right) - E(H_2O)\right] \quad \text{Eqn. (S4)}$$

Similarly, the reference state of $H^+C_4H_{10}O_6$ and H_2O was chosen because it is more stable than that of $C_4H_{10}O_6$ and H^+H_2O. In this case the binding energy is -53 kJ/mol.

Finally, for the m/z^+ 263 $H^+C_4H_8O_6\cdots C_2H_6O_5$, the binding energy was calculated using Eqn. (S5):

$$E_{binding} = \frac{1}{2}\left[E\left(H^+(C_4H_8O_6)(C_2H_6O_5)\right) - E\left(H^+(C_4H_8O_6)\right) - E(C_2H_6O_5)\right] \quad \text{Eqn. (S5)}$$

The reference state is chosen as $H^+C_4H_8O_6$ and $C_2H_6O_5$ because the proton only resides at $C_4H_8O_6$ in the MD simulation of this m/z^+ 263 ion, and the binding energy in this case is -70 kJ/mol.

Supporting Figures

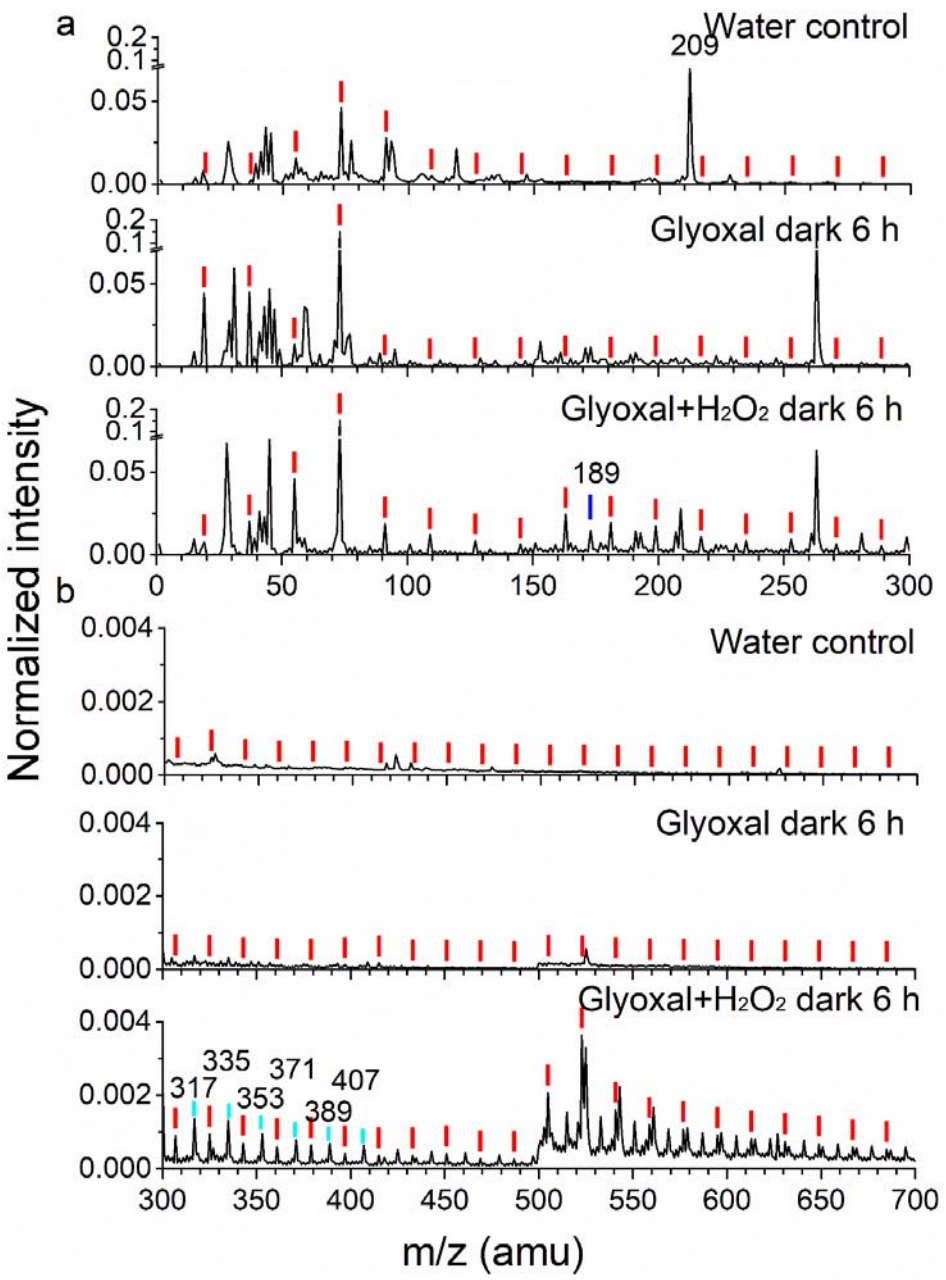

Fig. S1a. Liquid ToF-SIMS spectral comparison of water control, glyoxal and hydrogen peroxide, and the glyoxal control undergoing 6 hr. dark aging (a) in the mass to charge (m/z^+) range of 0 – 300 and (b) 300 – 700 in the positive ion mode, respectively. Red bars represent the locations of water cluster peaks, blue oligomers, and cyan cluster ions.

Fig. S1 supports additional in situ liquid SIMS spectral data to support Fig. 2 in the main text. Fig. S1 shows cluster ion formation in the dark aging samples when compared against the water control and glyoxal control after 6 hr. of aging in the negative mode.

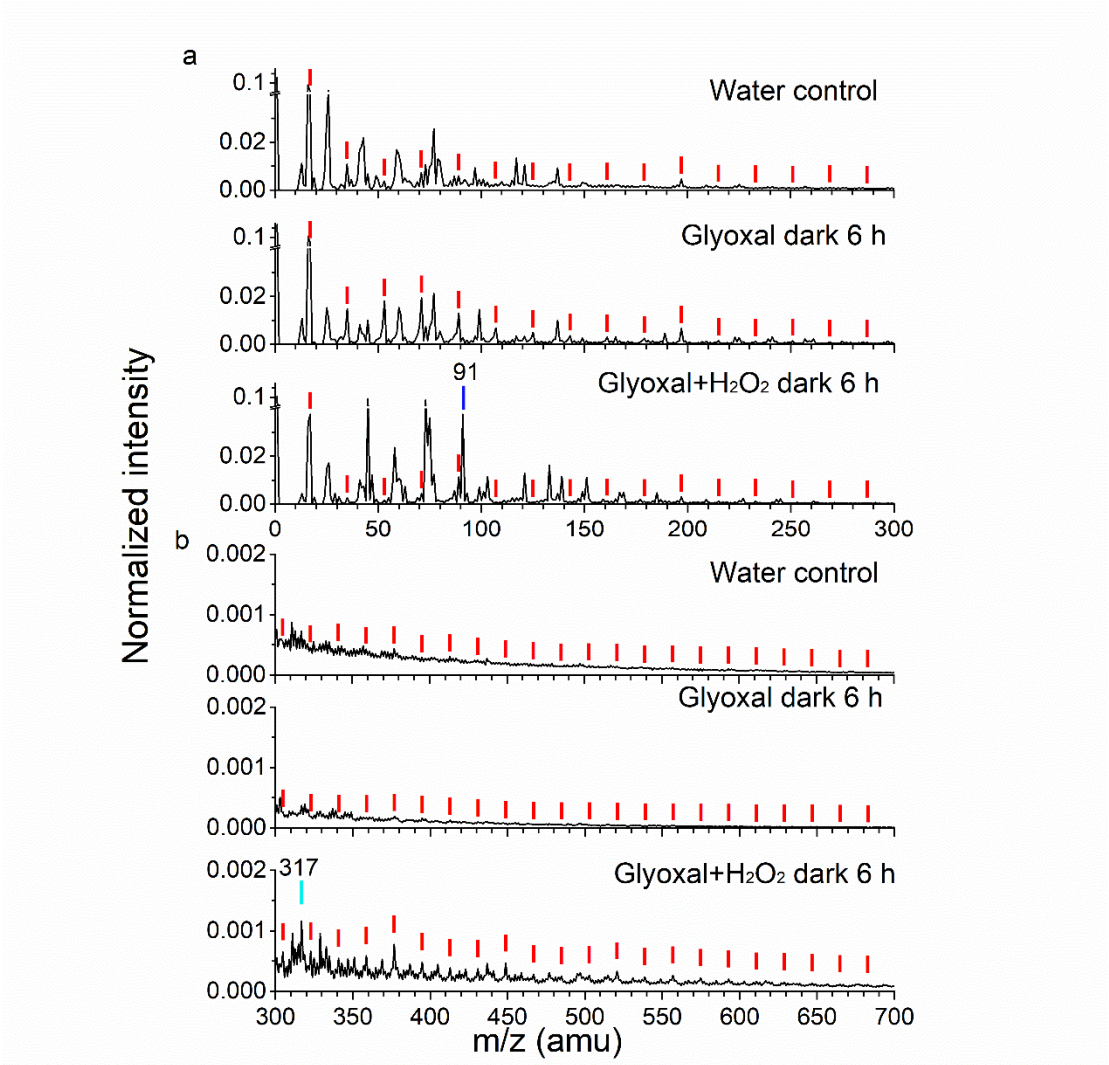

Fig. S1b. Liquid ToF-SIMS spectral comparison of water control, glyoxal and hydrogen peroxide, and the glyoxal control undergoing 6 hr. dark aging (a) in the m/z^- range of 0 – 300 and (b) 300 – 700 in the negative ion mode, respectively. Red bars represent the locations of water cluster peaks, blue oligomers, and cyan cluster ions.

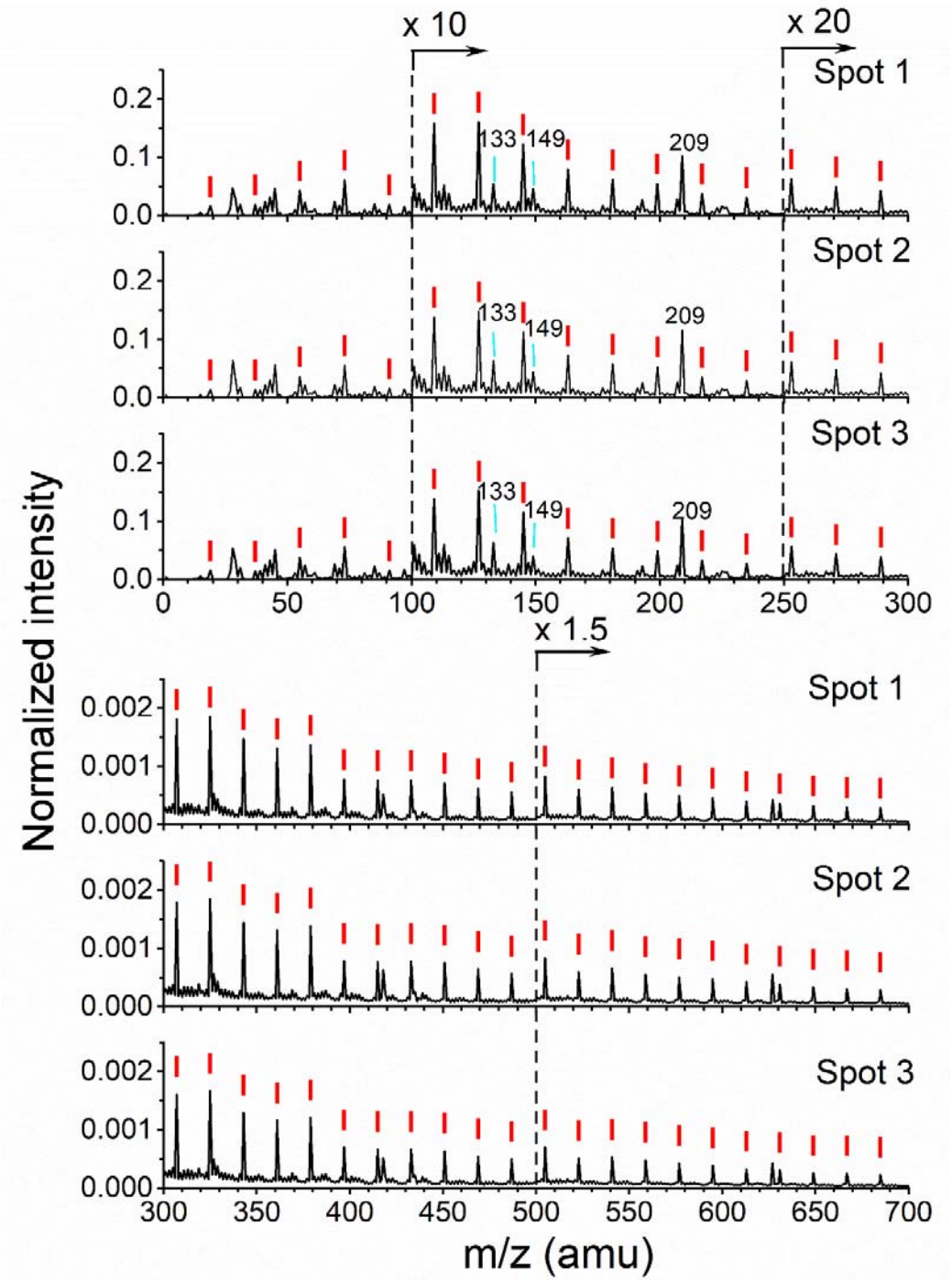

Fig. S2a. Liquid SIMS spectral reproducibility of 6 hr. UV aging in the positive ion mode (m/z^+ 1 – 700). Red color represents water clusters, green carboxylic acids, pink hydration products, blue oligomers, and cyan cluster ions.

Figs. S2a-d show the reproducibility of liquid ToF-SIMS measurement of the UV aging and dark aging results in the positive and negative mode. The measurement uncertainty of the experiments based on in situ liquid SIMS measurements is calculated using the following equation: Uncertainty = | Intensity of one spot- average intensity of 3 spots | / average intensity of 3 spots. The results are summarized in Table S2.

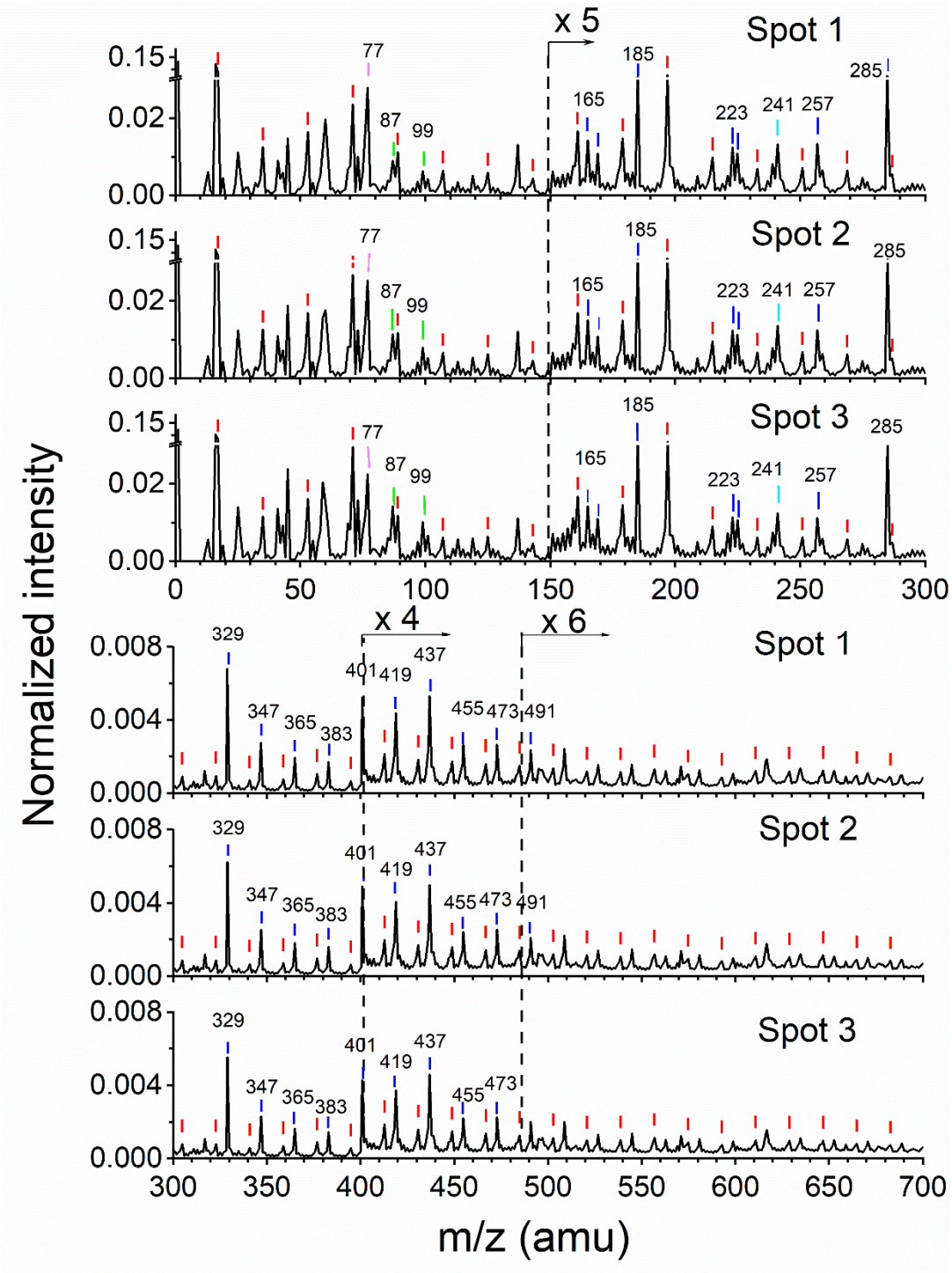

Fig. S2b. Liquid SIMS spectral reproducibility of 6 hr. UV aging in the negative ion mode (m/z^- 1 – 700). Red color represents water clusters, green carboxylic acids, pink hydration products, blue oligomers, and cyan cluster ions.

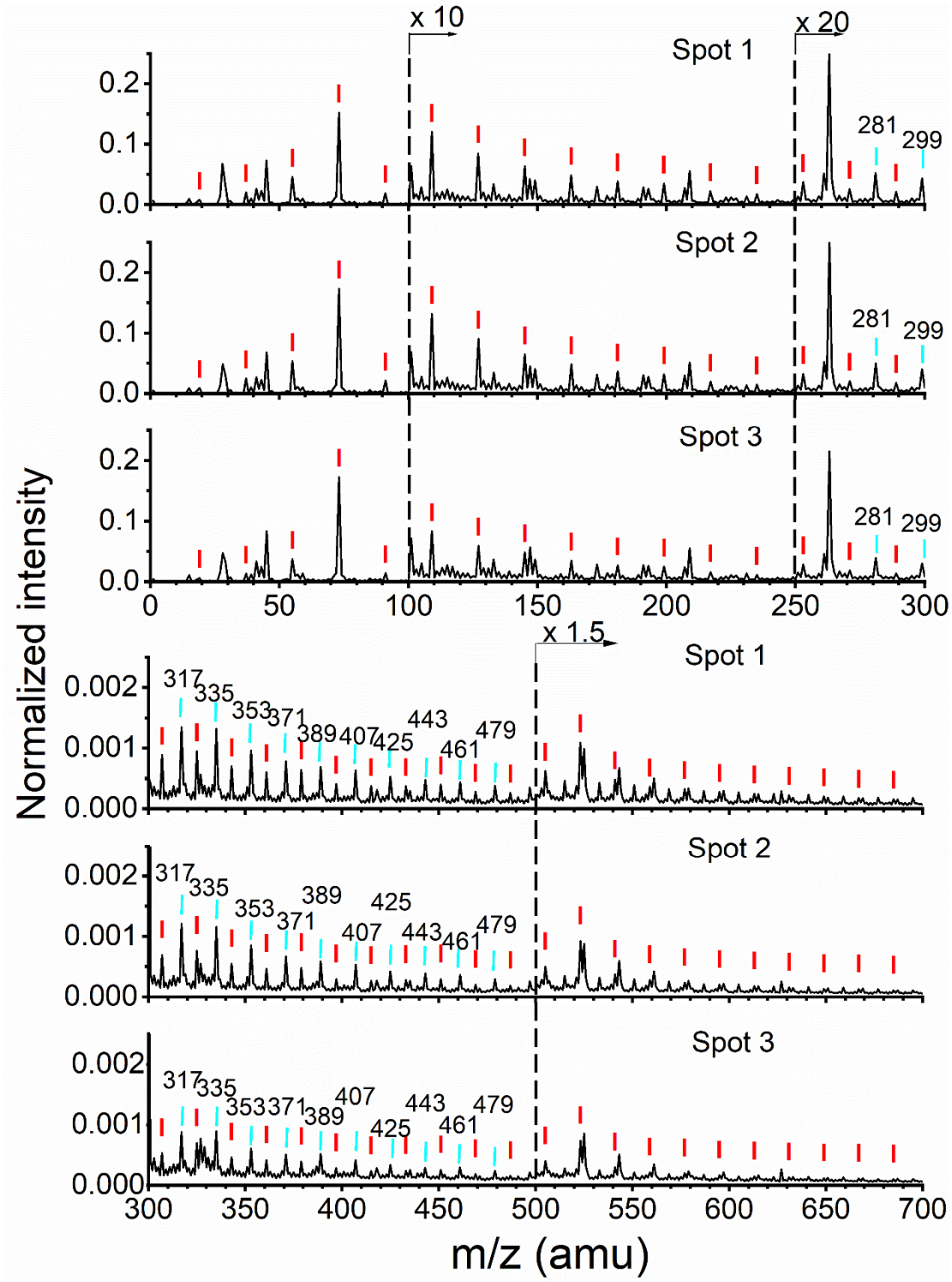

Fig. S2c. Liquid SIMS spectral reproducibility of 6 hr. dark aging in the positive ion mode (m/z^+ 1 – 700). Red color represents water clusters, green carboxylic acids, pink hydration products, blue oligomers, and cyan cluster ions.

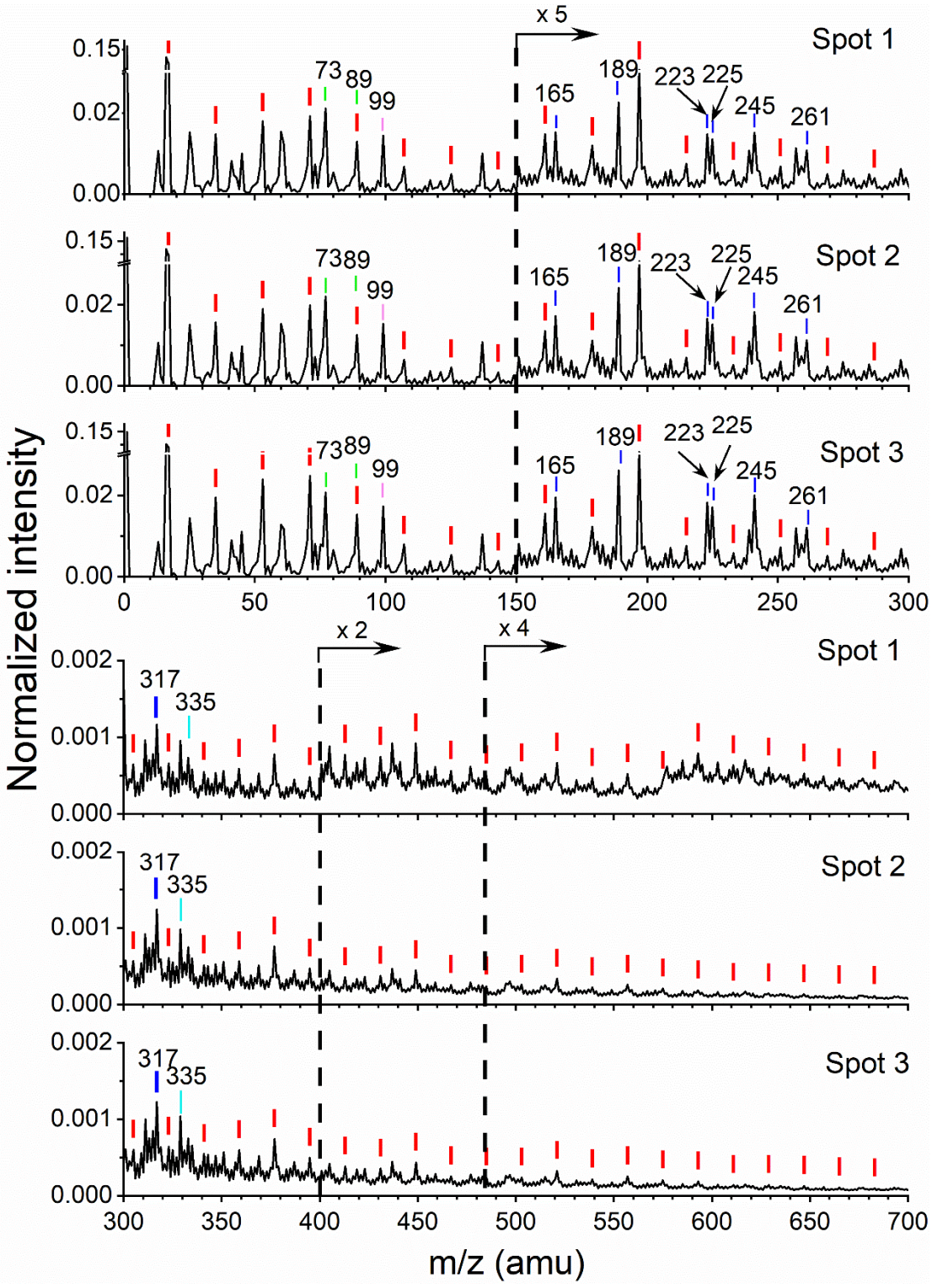

Fig. S2d. Liquid SIMS spectral reproducibility of 6 hr. dark aging in the negative ion mode (m/z^- 1 – 700). Red color represents water clusters, green carboxylic acids, pink hydration products, blue oligomers, and cyan cluster ions.

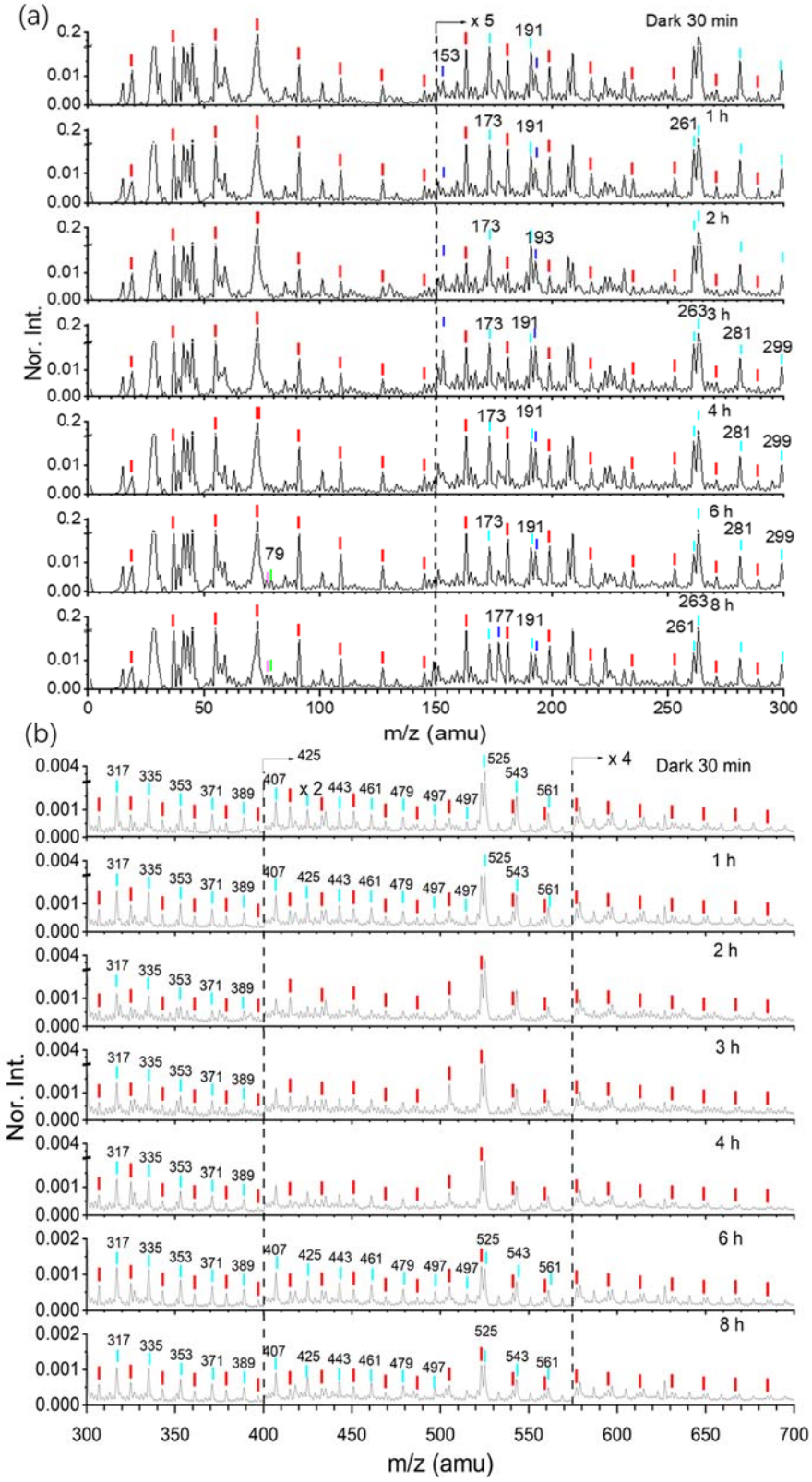

Fig. S3a. Comparison of all dark aging SIMS spectral data in the positive ion mode (a) m/z^+ 1 – 300 and (b) m/z^+ 300 – 700. Red color bars depict the location of water clusters, green carboxylic acids, pink hydration products, blue oligomers, and cyan cluster ions. All spectra were normalized to total ion intensities.

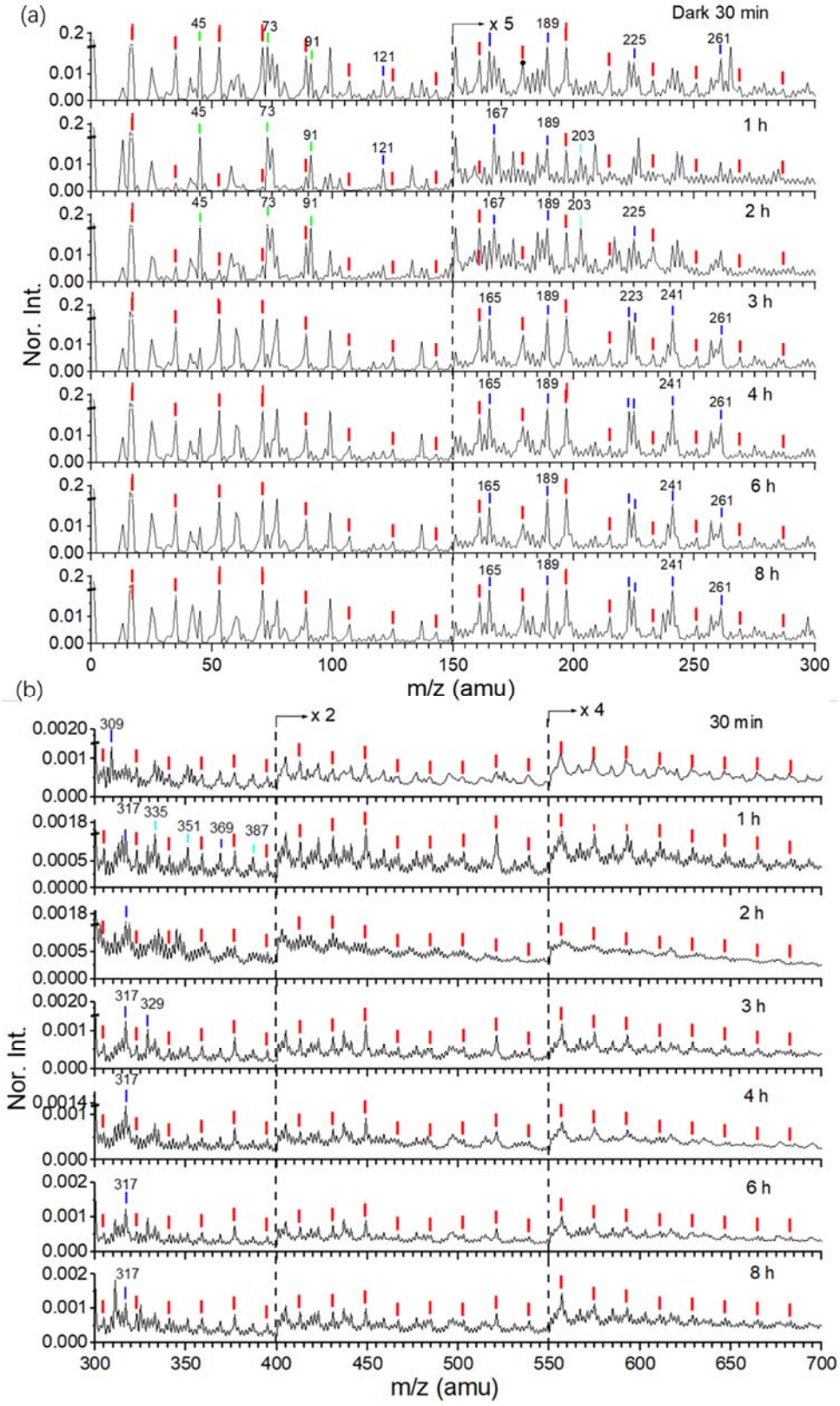

Fig. S3b. Comparison of all dark aging SIMS spectral data in the negative ion mode (a) m/z^- 1 – 300 and (b) m/z^- 300 – 700. Red color bars depict the location of water clusters, green carboxylic acids, pink hydration products, blue oligomers, and cyan cluster ions. All spectra were normalized to total ion intensities.

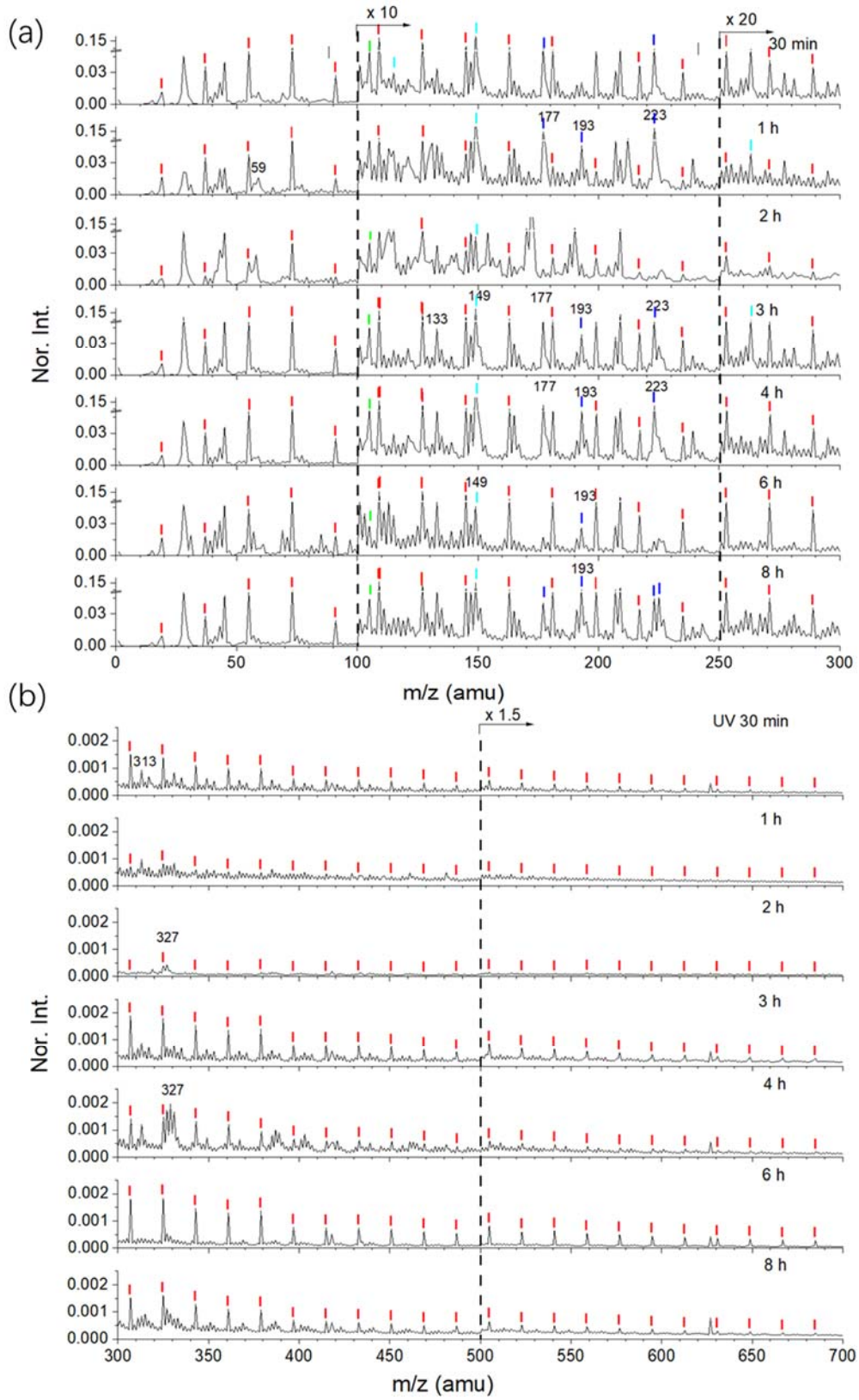

Fig. S3c. Comparison of all UV aging SIMS spectral data in the positive ion mode (a) m/z^+ 1 – 300 and (b) m/z^+ 300 – 700. Red color bars indicate water clusters, green carboxylic acids, pink hydration products, blue oligomers, and cyan color cluster ions. All the spectra were normalized to total ion intensities.

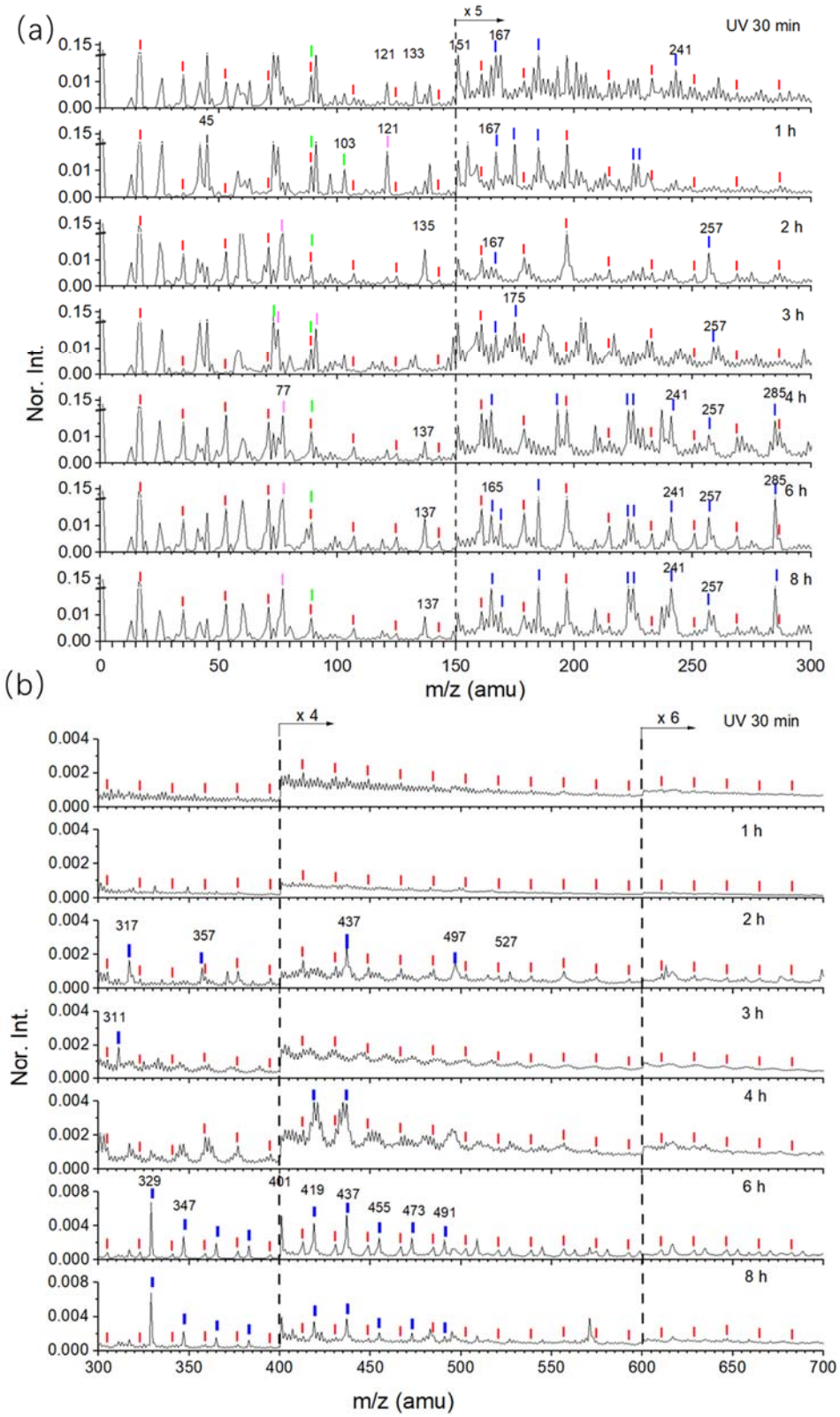

Fig. S3d. Comparison of all UV aging spectral data in the negative mode (a) m/z^- 1 – 300 and (b) m/z^- 300 – 700. Red color bars indicate water clusters, green carboxylic acids, pink hydration products, blue oligomers, and cyan color cluster ions. All spectra were normalized to total ion intensities.

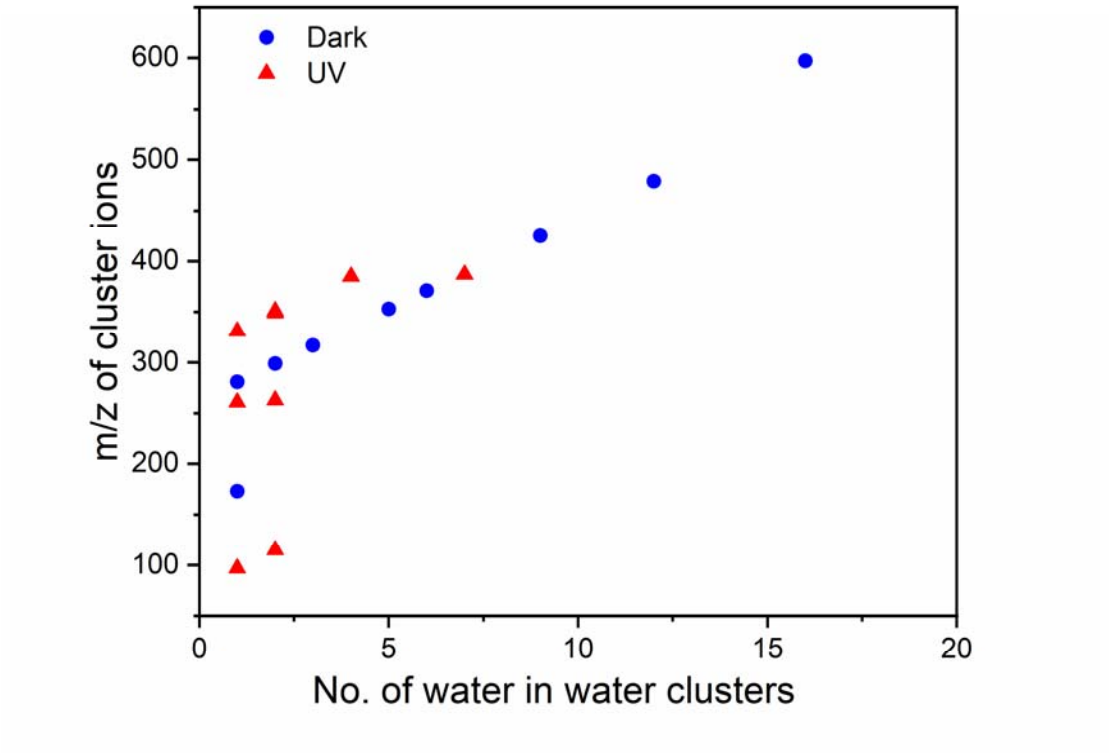

Fig. S4. Comparison of the trend between the number of water molecules in co-occurring water clusters and cluster ions in the UV and dark aging in the negative mode.

The x-axis of Fig. S3 represented the number of water molecules in the observed water clusters when there are co-occurring cluster ions from in situ liquid SIMS; and the y-axis represented the *m/z* s of the cluster ions observed in UV or dark aging. Fig. S3 shows that the water molecules are more likely to associate with organic molecules to form larger cluster ions during dark aging than UV aging. The small water clusters refer to $(H_2O)_nOH^-$ with n in the range of 1 to 16 in the negative mode and $(H_2O)_nH^+$ with n in the range of 1 to 17 in the positive mode in this work. The large water clusters refer to $(H_2O)_nOH^-$ with n in the range of 17 to 43 in the negative mode and $(H_2O)_nH^+$ with n in the range of 18 to 44 in this work.

Supporting Tables

Table S1. The sample matrices of the glyoxal and hydrogen peroxide oxidation experiments under UV and dark conditions.

Samples	Initial composition (mM)		Status	Aging time (h)	pH
	Glyoxal	H_2O_2			
UV aging					
1	5	20	Liquid	0.25	4.38
2			Liquid	0.5	4.15
3			Liquid	1	3.97
4			Liquid	2	3.86
5			Liquid	3	3.76
6			Liquid	4	3.70
7			Liquid	6	3.44
8			Liquid	8	3.21
Dark aging					
1	5	20	Liquid	0.5	4.5
2			Liquid	1	4.3
3			Liquid	2	3.99
4			Liquid	3	3.9
5			Liquid	4	3.74
6			Liquid	6	3.58
7			Liquid	8	3.45
Control					
1		20	Liquid	UV 2 hr.	8.45
2	5		Liquid	UV 2 hr.	4.46
3	5		Liquid	UV 6 hr.	4.43
4	5		Liquid	0	4.49
5		20	Liquid	0	8.45
6	5		Dry	0	4.49
7		20	Dry	0	8.45
8	Tartaric acid		Dry	neither UV nor dark	
9	Succinic acid		Dry	neither UV nor dark	
10	Malonic acid		Dry	neither UV nor dark	
11	Oxalic acid		Dry	neither UV nor dark	
12	Malic acid		Dry	neither UV nor dark	

Table S2. The liquid ToF-SIMS measurement uncertainties (%) of 6 hr. of glyoxal and hydrogen peroxide from UV and dark aging experiments.

UV aging			Dark aging		
oligomer	cluster ions	water cluster	oligomer	cluster ions	water cluster
Positive mode					
2.26	2.42	0.19	1.84	9.65	0.37
3.94	2.39	2.09	3.95	3.47	2.26
1.67	4.81	2.29	2.1	6.18	1.89
Negative mode					
3.12	2.11	3.44	3.64	2.12	0.85
3.11	1.75	1.08	1.99	1.26	0.32
0.01	0.36	4.52	1.66	0.86	0.53

Table S3. The main products identified in UV and dark aging in the positive ion mode.

m/z^+,	UV aging		Dark aging	
obs	$[M+H]^{+a}$	Possible assignment	$[M+H]^+$	Possible assignment
Oxidation products				
61	$C_2H_5O_2^+$	acetic acid		
91	$C_2H_3O_4^+$	oxalic acid		
119	$C_4H_7O_4^+$	succinic acid		
Oligomers/Polymers				
117	$C_4H_5O_4^+$	monohydrated glyoxal dimer		
231			$C_6H_{15}O_9^+$	m/z^+ 173 $C_4H_{13}O_7^+$— $C_2H_2O_2$ (glyoxal)[b]
239	$C_7H_{11}O_9^+$	$C_4H_6O_5$ (glyoxal dimer monohydrate)— $C_3H_4O_4$ (malonic acid)		
243	$C_6H_{11}O_{10}^+$	$C_4H_{10}O_6$ (dihydrated glyoxal dimer)— $C_2H_2O_4$ (oxalic acid)		
251	$C_8H_{11}O_9^+$	m/z^+ 177 $C_6H_9O_6^+$—$C_2H_4O_4$ (monohydrated glyoxylic acid)		
269	$C_8H_{13}O_{10}^+$	m/z^+ 251 $C_8H_{11}O_9^+$—H_2O		
285	$C_8H_{13}O_{11}^+$	m/z^+ 227 $C_6H_{11}O_9^+$— $C_2H_2O_2$ (glyoxal)		
313	$C_9H_{13}O_{12}^+$	m/z^+ 239 $C_7H_{11}O_9^+$— $C_2H_2O_3$ (glyoxylic acid)		
315	$C_9H_{15}O_{12}^+$	m/z^+ 269 $C_8H_{13}O_{10}^+$— CH_2O_2 (formic acid)		
329	$C_{10}H_{17}O_{12}^+$	m/z^+ 269 $C_8H_{13}O_{10}^+$—$C_2H_4O_2$ (acetic acid)		
401	$C_{12}H_{17}O_{15}^+$	m/z^+ 327 $C_{10}H_{15}O_{12}^+$— $C_2H_2O_3$ (glyoxylic acid)		
435	$C_{13}H_{23}O_{16}^+$	m/z^+ 285 $C_8H_{13}O_{11}^+$— $C_4H_6O_6$ (tartaric acid)		
461	$C_{11}H_{25}O_{19}^+$	m/z^+ 387 $C_9H_{23}O_{16}^+$— $C_2H_2O_3$ (glyoxylic acid)		
493	$C_{15}H_{25}O_{18}^+$	m/z^+ 435 $C_{13}H_{23}O_{16}^+$—$C_2H_2O_2$ (glyoxal)		
Cluster ions				
97	$C_2H_9O_4^+$	m/z^+ 79 $C_2H_7O_3^+\cdots H_2O$[c]		
115	$C_2H_{11}O_5^+$	m/z^+ 79 $C_2H_7O_3^+\cdots 2H_2O$		
149	$C_5H_9O_5^+$	m/z^+ 131 $C_5H_7O_4^+\cdots H_2O$		
165	$C_4H_5O_7^+$	glyoxylic acid$\cdots C_2H_2O_4$ (oxalic acid)		

m/z^+,	UV aging		Dark aging	
obs	$[M+H]^{+a}$	Possible assignment	$[M+H]^+$	Possible assignment
281	$C_6H_{17}O_{12}^+$	m/z^+ 263 $C_6H_{15}O_{11}^+\cdots H_2O$	$C_6H_{17}O_{12}^+$	m/z^+ 263 $C_6H_{15}O_{11}^+\cdots H_2O$
331	$C_9H_{15}O_{13}^+$	m/z^+ 313 $C_9H_{13}O_{12}^+\cdots H_2O$		
341	$C_{10}H_{13}O_{13}^+$	m/z^+ 251 $C_8H_{11}O_9^+\cdots$ $C_2H_2O_4$ (oxalic acid)		
349	$C_9H_{17}O_{14}^+$	m/z^+ 313 $C_9H_{13}O_{12}^+\cdots 2H_2O$		
351	$C_9H_{19}O_{14}^+$	m/z^+ 315 $C_9H_{15}O_{12}^+$ $\cdots 2H_2O$		
367	$C_9H_{19}O_{15}^+$	m/z^+ 313 $C_9H_{13}O_{12}^+\cdots 3H_2O$		
369	$C_9H_{21}O_{15}^+$	m/z^+ 315·$C_9H_{15}O_{12}^+\cdots 3H_2O$		
385	$C_9H_{21}O_{16}^+$	m/z^+ 313 $C_9H_{13}O_{12}^+\cdots 4H_2O$		
387	$C_9H_{23}O_{16}^+$	m/z^+ 315 $C_9H_{15}O_{12}^+\cdots 4H_2O$		
421	$C_{11}H_{17}O_{17}^+$	m/z^+ 331 $C_9H_{15}O_{13}^+\cdots C_2H_2O_4$ (oxalic acid)		
445	$C_{11}H_{25}O_{18}^+$	m/z^+ 387 $C_9H_{15}O_{12}^+\cdots$glyoxal		
511	$C_{15}H_{27}O_{19}^+$	m/z^+ 493 $C_{15}H_{25}O_{18}^+\cdots H_2O$		
515			$C_6H_{43}O_{26}^+$	m/z^+ 263 $C_6H_{15}O_{11}^+\cdots 14H_2O$
525			$C_7H_{41}O_{25}^+$	m/z^+ 479 $C_6H_{39}O_{23}^+\cdots CH_2O_2$ (formic acid)
543			$C_7H_{43}O_{26}^+$	m/z^+ 525 $C_7H_{41}O_{25}^+\cdots H_2O$
551			$C_6H_{47}O_{28}^+$, $C_{14}H_{31}O_{22}^+$	m/z^+ 533 $C_6H_{45}O_{27}^+$, $C_{14}H_{29}O_{21}\cdots H_2O$
561			$C_7H_{45}O_{27}^+$	m/z^+ 525 $C_7H_{41}O_{25}^+\cdots 2H_2O$
579			$C_7H_{47}O_{28}^+$	m/z^+ 525 $C_7H_{41}O_{25}^+\cdots 3H_2O$
597			$C_7H_{49}O_{29}^+$	m/z^+ 525 $C_7H_{41}O_{25}^+\cdots 4H_2O$

[a] Peak assignment uses the peak center to estimate the major component.

[b] This "—" symbol represents the covalent bond formed by chemical reactions.

[c] This "···" symbol represents the van der Waals force, hydrogen bonds, and other weak intermolecular forces between molecules.

Table S4. The main products identified in dark and UV aging in the negative ion mode.

m/z^-, obs	UV aging		Dark aging	
	$[M-H]^-$	Possible assignment	$[M-H]^-$	Possible assignment
Oxidation products				
45	CHO_2^-	formic acid	CHO_2^-	formic acid
73	$C_2HO_3^-$	glyoxylic acid	$C_2HO_3^-$	glyoxylic acid
75	$C_2H_3O_3^-$	glycolic acid		
89	$C_2HO_4^-$	oxalic acid	$C_2HO_4^-$	oxalic acid
91			$C_2H_3O_4^-$	HHPE (Zhao et al., 2012)
103	$C_3H_3O_4^-$	malonic acid		
117	$C_4H_5O_4^-$	succinic acid		
133	$C_4H_5O_5^-$	malic acid		
149	$C_4H_5O_6^-$	tartaric acid		
Oligomers/Polymers				
161	$C_5H_5O_6^-$	$C_3H_4O_5$ (malonic acid)—$C_2H_4O_3$ (monohydrated glyoxal)/$C_2H_2O_4$ (oxalic acid)—$C_2H_2O_4$ (oxalic acid)		
169	$C_4H_9O_7^-$	$C_2H_4O_3$ (monohydrated glyoxal)—$C_2H_6O_4$ (dihydrated glyoxal)		
179	$C_5H_7O_7^-$	$C_3H_4O_5$ (malonic acid)—$C_2H_6O_4$ (dihydrated glyoxal)		
185			$C_4H_9O_8^-$	m/z^- 110 $C_2H_6O_5$[c]—m/z 76 $C_2H_4O_3$[d]
189			$C_6H_5O_7^-$	m/z^- 116 $C_4H_3O_4^-$—m/z 74 $C_2H_2O_3$
193			$C_5H_5O_8^-$	m/z^- 120 $C_3H_4O_5$—m/z^- 74 $C_2H_2O_3$
209	$C_6H_9O_8^-$	m/z^- 133 $C_4H_5O_5^-$—$C_2H_4O_3$ (monohydrated glyoxal)		
217			$C_4H_9O_{10}^-$	m/z^- 126 $C_2H_5O_6$—m/z 92 $C_2H_4O_4$
223	$C_6H_7O_9^-$	$C_4H_6O_5$ (monohydrated glyoxal dimer)—$C_2H_2O_4$ (oxalic acid)	$C_6H_7O_9^-$	monohydrated glyoxal dimer—$C_2H_2O_4$ (oxalic acid)
237	$C_6H_5O_{10}^-$	m/z^- 165 $C_4H_5O_7^-$— $C_2H_2O_4$ (oxalic acid)		
239			$C_6H_7O_{10}^-$	m/z^- 74 $C_2H_2O_3^-$—m/z 74 $C_2H_2O_3$—m/z 92 $C_2H_4O_4$

m/z^-, obs	UV aging		Dark aging	
	$[M-H]^-$	Possible assignment	$[M-H]^-$	Possible assignment
249	$C_8H_9O_9^-$	4 $C_2H_4O_3$ (monohydrated glyoxal)		
261			$C_6H_{13}O_{11}^-$	*m/z*$^-$ 110 $C_2H_6O_5^-$—*m/z* 76 $C_2H_4O_3$—*m/z* 76 $C_2H_4O_3$
283	$C_8H_{11}O_{11}^-$	$C_4H_6O_6$ (monohydrated tartaric acid)— $C_4H_6O_5$ malic acid		
285	$C_8H_{13}O_{11}^-$	$C_6H_{12}O_9$ (dihydrated glyoxal trimer)— $C_2H_2O_2$ (glyoxal)		
299	$C_8H_{11}O_{12}^-$	$C_2H_4O_3$ (monohydrated glyoxal)— $C_2H_2O_3$ (glyoxylic acid)— $C_4H_6O_6$ (tartaric acid)		
303			$C_7H_{11}O_{13}^-$	*m/z*$^-$ 257 $C_6H_9O_{11}CH_2O_2$ (formic acid)
307			$C_6H_{11}O_{14}^-$	*m/z*$^-$ 126 $C_2H_5O_6$— *m/z* 90 $C_2H_2O_4$— *m/z*$^-$ 92 $C_2H_4O_4$
309			$C_6H_{13}O_{14}^-$	*m/z*$^-$ 126 $C_2H_5O_6$— *m/z* 92 $C_2H_4O_4$— *m/z* 92 $C_2H_4O_4$
311	$C_9H_{11}O_{12}^-$	*m/z*$^-$ 237 $C_6H_5O_{10}^-$— $C_2H_2O_3$ (glyoxylic acid)/*m/z*$^-$ 161 $C_5H_5O_6^-$— $C_4H_6O_6$ (tartaric acid)		
317	$C_8H_{13}O_{13}^-$	$C_2H_4O_3$ (monohydrated glyoxal)—$C_2H_2O_3$ (glyoxylic acid)—$C_4H_8O_7$ (monohydrated tartaric acid)		
329	$C_9H_{13}O_{13}^-$	*m/z*$^-$ 311 $C_9H_{11}O_{12}^-$—H_2O		
343	$C_{10}H_{15}O_{13}^-$	$C_4H_8O_7$ (monohydrated tartaric acid)—$C_4H_8O_5$ (monohydrated malic acid)—$C_2H_4O_2$ (acetic acid)		
357	$C_{10}H_{13}O_{14}^-$	2 $C_2H_4O_3$ (monohydrated glyoxal)—$C_2H_2O_3$ (glyoxylic acid)—$C_4H_8O_7$ (monohydrated tartaric acid)		
359	$C_{10}H_{15}O_{14}^-$	$C_4H_6O_5$ (malic acid)—$C_2H_3O_3$ (glycolic acid)/$C_4H_5O_6$ (tartaric acid)$\cdots 3H_2O$		
377	$C_{10}H_{17}O_{15}^-$	*m/z*$^-$ 359 $C_{10}H_{15}O_{14}^-\cdots H_2O$		
383	$C_{12}H_{15}O_{14}^-$	6 glyoxal dihydrate		
401	$C_{12}H_{17}O_{15}^-$	5 glyoxal dihydrate—monohydrated glyoxal		

m/z^-, obs	UV aging		Dark aging	
	$[M-H]^-$	Possible assignment	$[M-H]^-$	Possible assignment
419	$C_{12}H_{19}O_{16}^-$	4 glyoxal dihydrate—2 monohydrated glyoxal		
421	$C_{14}H_{13}O_{15}^-$	6 glyoxal—monohydrated glyoxal		
437	$C_{12}H_{21}O_{17}^-$	glyoxal—5 monohydrated glyoxal		
455	$C_{12}H_{23}O_{18}^-$	6 monohydrated glyoxal		
473	$C_{12}H_{25}O_{19}^-$	5 monohydrated glyoxal—dihydrated glyoxal		
491	$C_{12}H_{27}O_{20}^-$	4 monohydrated glyoxal—2 dihydrated glyoxal		
499	$C_{16}H_{19}O_{18}^-$	6 glyoxal—2 monohydrated glyoxal		
509	$C_{12}H_{29}O_{21}^-$	3 monohydrated glyoxal—3 dihydrated glyoxal		
527	$C_{12}H_{31}O_{22}^-$	2 monohydrated glyoxal—4 dihydrated glyoxal		
545	$C_{12}H_{33}O_{23}^-$	1 monohydrated glyoxal—5 dihydrated glyoxal		
557	$C_{18}H_{21}O_{20}^-$	7 glyoxal—2 monohydrated glyoxal		
Cluster ions				
63			$CH_3O_3^-$	m/z^- 45 $CHO_2^-\cdots H_2O$[b]
139			$C_2H_3O_7^-$	m/z^- 121 $C_2HO_6^-\cdots H_2O$
241	$C_6H_9O_{10}^-$	m/z^- 223 $C_6H_7O_9^-\cdots H_2O$[b]		
269	$C_7H_9O_{11}^-$	2 $C_2H_2O_4$ (oxalic acid)$\cdots C_3H_4O_2$ (hydroxy acids)$\cdots H_2O$/m/z^- 99 $C_3O_5^-\cdots$ m/z^- 133 $C_4H_5O_5^-\cdots 2H_2O$		
335			$C_6H_{17}O_{16}^-$	m/z^- 317 $C_6H_{15}O_{15}^-\cdots H_2O$
359	$C_{10}H_{15}O_{14}^-$	$C_4H_6O_5$ (malic acid)—$C_2H_4O_3$ (glycolic acid)—$C_4H_6O_6$ (tartaric acid)$\cdots 3H_2O$		
617	$C_{20}H_{25}O_{22}^-$	m/z^- 557 $C_{18}H_{21}O_{20}^-\cdots C_2H_4O_2$ (acetic acid)		
635	$C_{19}H_{23}O_{24}^-$	m/z^- 617 $C_{20}H_{25}O_{22}^-\cdots H_2O$		

[a] Peak assignment uses the peak center to estimate the major component.

[b] This "—" symbol represents the van der Waals force, hydrogen bonds, and other weak intermolecular forces between molecules.

[c] This "…" symbol represents the covalent bond formed by chemical reactions.

Table S5. The calculated binding energy of representative cluster ions using AIMD simulations.

m/z^+	Possible peak assignment	Binding energy per molecule (kJ/mol)
55	$H^+H_2O_3$	-81
109	$H^+H_2O_6$	-70
113	$H^+H_2O_3\cdots C_2H_2O_2$	-84
165	$H^+C_2H_3O_3\cdots C_2H_2O_4$	-62
173	$H^+C_4H_{10}O_6\cdots H_2O$	-53
263	$H^+C_4H_8O_6\cdots C_2H_6O_5$	-70

References

Adamo, C., Barone, V., 1999. Toward reliable density functional methods without adjustable parameters: The PBE0 model. J Chem Phys 110, 6158-6170.

Bruny, G., Eden, S., Feil, S., Fillol, R., El Farkh, K., Harb, M.M., Teyssier, C., Ouaskit, S., Abdoul-Carime, H., Farizon, B., Farizon, M., Mark, T.D., 2012. A new experimental setup designed for the investigation of irradiation of nanosystems in the gas phase: A high intensity mass-and-energy selected cluster beam. Rev. Sci. Instrum. 83, 013305.

Hirata, S., Head-Gordon, M., 1999. Time-dependent density functional theory within the Tamm-Dancoff approximation. Chem. Phys. Lett. 314, 291-299.

Pritchard, B.P., Altarawy, D., Didier, B., Gibson, T.D., Windus, T.L., 2019. New Basis Set Exchange: An Open, Up-to-Date Resource for the Molecular Sciences Community. J Chem Inf Model 59, 4814-4820.

Sosnik, A., Sodhi, R.N.S., Brodersen, P.M., Sefton, M.V., 2006. Surface study of collagen/poloxamine hydrogels by a 'deep freezing' ToF-SIMS approach. Biomaterials 27, 2340-2348.

Sui, X., Zhou, Y.F., Zhang, F., Chen, J.M., Zhu, Z.H., Yu, X.Y., 2017. Deciphering the aqueous chemistry of glyoxal oxidation with hydrogen peroxide using molecular imaging. Phys Chem Chem Phys 19, 20357-20366.

Sui, X., Zhou, Y.F., Zhang, F., Zhang, Y.Y., Chen, J.M., Zhu, Z.H., Yu, X.Y., 2018. ToF-SIMS characterization of glyoxal surface oxidation products by hydrogen peroxide: A comparison between dry and liquid samples. Surf. Interface Anal. 50, 927-938.

Vaida, V., 2011. Perspective: Water cluster mediated atmospheric chemistry. J. Chem. Phys. 135, 020901.

Valiev, M., Bylaska, E.J., Govind, N., Kowalski, K., Straatsma, T.P., Van Dam, H.J.J., Wang, D., Nieplocha, J., Apra, E., Windus, T.L., de Jong, W., 2010. NWChem: A comprehensive and scalable open-source solution for large scale molecular simulations. Comput. Phys. Commun. 181, 1477-1489.

VandeVondele, J., Krack, M., Mohamed, F., Parrinello, M., Chassaing, T., Hutter, J., 2005. QUICKSTEP: Fast and accurate density functional calculations using a mixed Gaussian and plane waves approach. Comput. Phys. Commun. 167, 103-128.

Verlet, J.R.R., Bragg, A.E., Kammrath, A., Cheshnovsky, O., Neumark, D.M., 2005. Observation of large water-cluster anions with surface-bound excess electrons. Science 307, 93-96.

Verlet, L., 1967. Computer Experiments on Classical Fluids .I. Thermodynamical Properties of Lennard-Jones Molecules. Phys Rev 159, 98-103.

Yang, L., Yu, X.-Y., Zhu, Z., Thevuthasan, T., Cowin, J.P., 2011a. Making a hybrid microfluidic platform compatible for in situ imaging by vacuum-based techniques. J. Vac. Sci. Technol. A 29, 061101.

Yang, L., Yu, X.Y., Zhu, Z.H., Iedema, M.J., Cowin, J.P., 2011b. Probing liquid surfaces under vacuum using SEM and ToF-SIMS. Lab Chip 11, 2481-2484.

Zhang, F., Yu, X., Chen, J., Zhu, Z., Yu, X.-Y., 2019a. Dark air–liquid interfacial chemistry of glyoxal and hydrogen peroxide. npj Clim. Atmos. Sci. 2, 28.

Zhang, F., Yu, X.F., Sui, X., Chen, J.M., Zhu, Z.H., Yu, X.Y., 2019b. Evolution of aqSOA from the Air-Liquid Interfacial Photochemistry of Glyoxal and Hydroxyl Radicals. Environ Sci Technol 53, 10236-10245.
Zhao, R., Lee, A.K.Y., Abbatt, J.P.D., 2012. Investigation of Aqueous-Phase Photooxidation of Glyoxal and Methylglyoxal by Aerosol Chemical Ionization Mass Spectrometry: Observation of Hydroxyhydroperoxide Formation. J. Phys. Chem. A 116, 6253-6263.